# Ambient noise correlation study at the CaMI Field Research Station, Newell County, Alberta, Canada

Marie Macquet and Don C. Lawton

## ABSTRACT

We recorded passive continuous seismic data at the CaMI Field Research Station to study the feasibility of using ambient noise correlation method as an additional tool to monitor and verify secure storage of the injected $CO_2$. In this paper, we focus on two aspects: (1) the near surface tomography, using 112 stations along the 1.1 km trench and (2) the long-term monitoring of the velocity change using continuous recording since October 2014 on 7 broadband stations. Due to the frequency range of the geophones used for the tomography part, the investigation depth remains shallow (up to 50 m depth). Nevertheless, a good near-surface velocity model remains important for active seismic processing. The $V_S$ model obtained with ambient noise correlation method is similar to the one obtained from an active shear seismic source study (bedrock depth and $V_S$ range).

Concerning the monitoring using the ambient noise correlation method, the daily correlations between 2 broadband stations show good coherency. The velocity variation between the daily correlations and the reference are obtained using Moving Window Cross Spectrum analysis on the daily correlations. The effect of the seasonal temperature is clearly visible on the velocity variation curves. We also suspect an effect of the $CO_2$ injection. Further analysis is required to confirm the first observations.

## INTRODUCTION

Reducing GHG emissions and climate impacts is a major global challenge. $CO_2$ capture, utilization and storage, with an emphasis on post-combustion capture and storage in geological media is a successful and important method for achieving international commitments (Mac Dowell et al., 2017). Several large-scale projects demonstrate the potential of capture and storage solutions, such as Aquistore in Canada (Rostron et al., 2014), Sleipner in Norway (Arts et al., 2008) or Ketzin in Germany (Bergmann et al., 2013). The development of the plume as well as the integrity of the cap-rock are highly monitored during the life cycle of a $CO_2$ storage site.

In this paper, we propose to study the feasibility of using the ambient noise correlation method as an innovative and additional tool to monitor the gas injection and plume monitoring. Continuous seismic data are already recorded and use for events detections. The ambient noise correlation method uses the same continuous seismic record and allows to turn any receiver into a virtual source, so we can approximate the Green's function between two receivers without using active sources. The fact that it is not using any active source reduce the survey cost and the fact that it is using continuous seismic data allows a true continuous monitoring that may be able to detect the transient changes of the subsurface. On the other hand, not using active source decreases the quality of the data such as body waves retrieval, and even if improvements are done with time, the ambient noise correlation method does not reach the imaging results that can be achieve by active surveys.

The CaMI Field Research Station is a pilot $CO_2$ storage site built to asset and develop monitoring tool to ensure the safety of $CO_2$ storage. As a small amount of $CO_2$ is planned to be injected for that project, it will be challenging to test the ambient noise method.

In this paper, we first give an overview of the CaMI Field Research Station and its instrumentation. We then present the available dataset and the ambient noise correlation method. The tomography of the near surface and the first results on monitoring using the ambient noise correlation method are presented and discussed.

## CAMI.FRS

The Containment and Monitoring Institute (CaMI) of CMC Research Institutes Inc., in collaboration with the University of Calgary, has developed a comprehensive Field Research Station (FRS) in southern Alberta, Canada, located 200km SE of Calgary (Figure 1). One of the purposes of the CaMI.FRS is to develop early monitoring technologies for potential $CO_2$ leakage. To reach that goal, we are injecting small and controlled amount of $CO_2$ at shallow depth (Basal Belly River Sandstone Formation - 300m depth, Fig. 1).

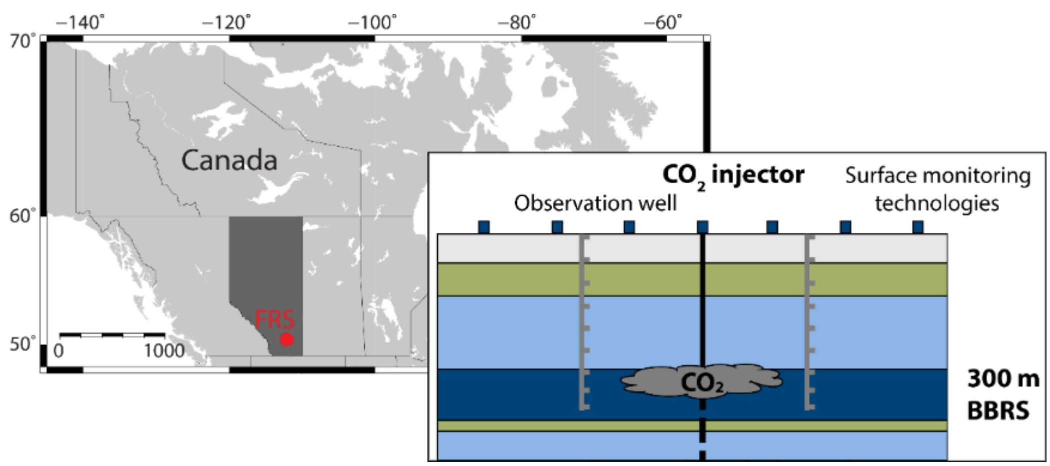


FIG. 1. Location and schematic of the CaMI Field Research Station near Brooks, AB (Canada). BBRS: Basal Belly River Sandstones is the injection target.

Several geophysical and geochemical are installed permanently at the FRS, including:

- a 3D array of 3C geophones (Lawton et al., 2015b);
- 3 permanent mounted vibratory sources (Spackman and Lawton, 2017, 2018);
- 5km of distributed acoustic sensing (DAS) using straight and helical fiber optical cables deployed in a 1.1km horizontal trench and in 2 observation wells (Gordon and Lawton, 2017, 2018; Hall et al., 2017, 2018);
- a permanent array of 128 electrodes for electrical resistivity tomography buried in the 1.1km trench and in one observation well;
- 7 broadband seismic stations (Storke et al., 2018).

In addition to the permanent equipment, several geophysical experiments were and will be conducted at the FRS, including:

- 2D and 3D surface seismic surveys (Isaac and Lawton, 2017);
- Vertical Seismic Surveys (VSP) (Gordon et al., 2016; Hall et al., 2015, 2018);
- cross well seismic and electromagnetic surveys (Marchesini et al., 2018, 2019);
- punctual electric resistivity tomography surveys (Rippe et al., 2017, 2016);
- magnetometric resistivity surveys (Bouchedda and Giroux, 2016).

At least two of each were acquired during the baseline time (without injection)to characterized the subsurface and to avoid using only one dataset that can be biased by whatever reason.

## SEISMIC BACKGROUND STUDIES

### Surface seismic

In May 2014, the 3D-3D baseline survey was shot (Lawton et al., 2015a). The processed volume (Isaac and Lawton, 2015) was used to build the geostatic model of the Field Research Station (Dongas, 2016) and will be used as reference for seismic time lapse studies.

In their paper, Macquet et al. (2019) studied the feasibility of time-lapse seismic monitoring at the Field Research Station by including the effect of the changes in $CO_2$ saturation but also the effect of the pressure changes. The first has effect on the fluid properties whereas the second has noticeable effect on the rock properties. Figure 2 shows the range of changes in elastic parameters expected at the FRS as function of the $CO_2$ saturation of the pore pressure. Table 1 resumes the variation in elastic parameters expected at the FRS after 5 years of continuous injection, taking account the effect of the $CO_2$ saturation only, pressure effect only or the combination of both.

| | Saturation only | Pressure only | Saturation and Pressure |
|---|---|---|---|
| $V_P$ variation | -24.5% | -7.5% | -35.7% |
| $V_P$ variation | 0.5% | -21.3% | -21% |
| $\rho$ variation | -1.1% | 0% | -0.7% |

Table 1. Variation in elastic parameters.

Macquet et al. (2019) show that using surface conventional surface seismic technique with the 2014 inner survey layout, we expect to detect the plume after 266 tonnes of injected $CO_2$ (or 1 year at ideal continuous injection rate), which set up the time frame for next big 3D active seismic acquisition. They also showed the strong effect that pressure can have, especially on the S-wave velocity.

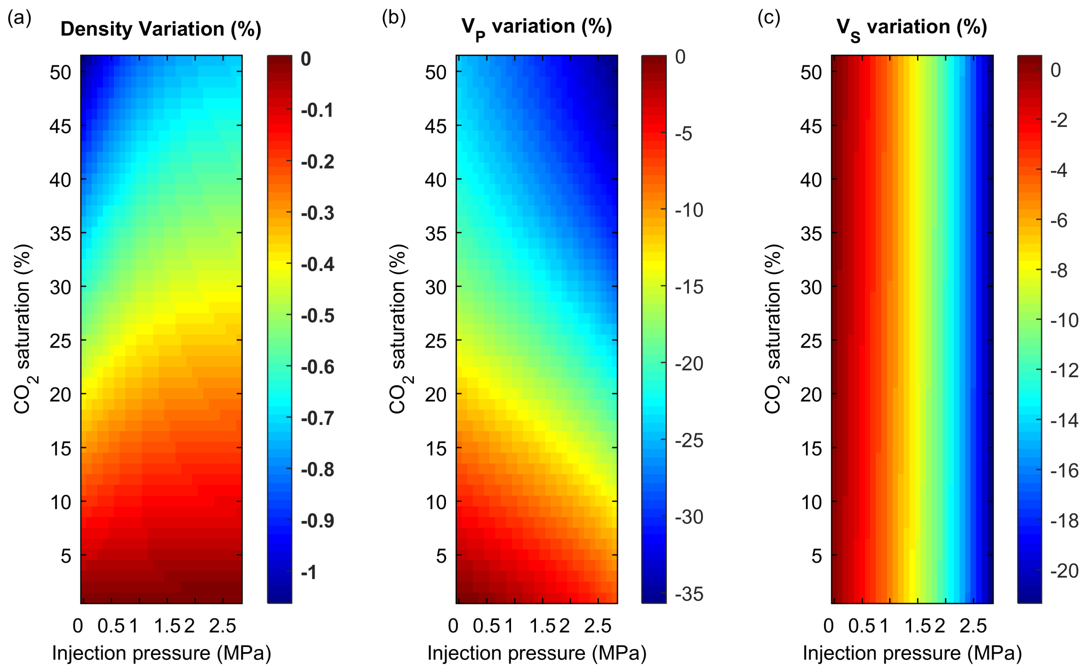


FIG. 2. Elastic parameters variation as function of CO2 saturation and pore pressure. (a) Density, (b) P-wave velocity, (c) S-wave velocity, from Macquet et al. (2019).

## Vertical Seismic Profiles

In addition to the DAS fiber, the geophysics monitoring well contains 24 3C geophones that can be used for techniques comparison. In her thesis work, Gordon (2019) shows the processing used for VSP DAS and geophones analysis.

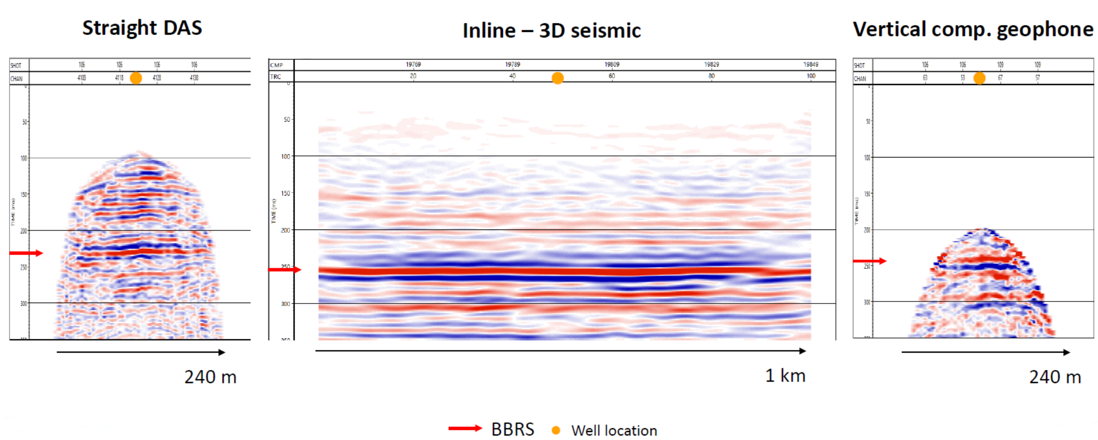


FIG. 3. Comparison between straight fiber, baseline surface seismic and downhole geophones, from Gordon and Lawton (2019). BBRS is Basal Belly River Sandstone corresponding to the injection target.

Figure 3 shows a comparison between DAS data, 3D surface seismic from 2016 and downhole geophones. We can observe a good coherency between the 3 dataset, with a strong reflector corresponding the injection zone (BBRS). The full coverage of the fiber optic cable in the well yields to better imaging in the shallow section.

## Permanently installed seismic sources

Three permanent sources are installed at the Field Research Station (Spackman and Lawton, 2018). Table 2 summarizes the 3 sources. The downhole linear vibrator it buried in a 15m deep well. The helical pile is 30m deep and its purpose is to transfer energy from the source to the anchor point at the end of the pile, thus allowing the source signature to bypass the attenuative near-surface layer.

| source name | Frequency range | Peak force (lbs.) |
|---|---|---|
| Downhole linear vibrator | 0-200 | 4500 |
| Surface linear vibrator | 0-200 | 4500 |
| Surface linear vibrator (on helical pile) | 0-100 | 11000 |

Table 2. Permanent sources parameters.

Figure 4 shows a comparison of the corridor stack using the downhole geophones using the downhole linear vibrator and the Vibroseis truck as sources. We can see an excellent comparison between the two sources. Having a permanently installed source on the site reduces the repeatability issues that active surveys may have.

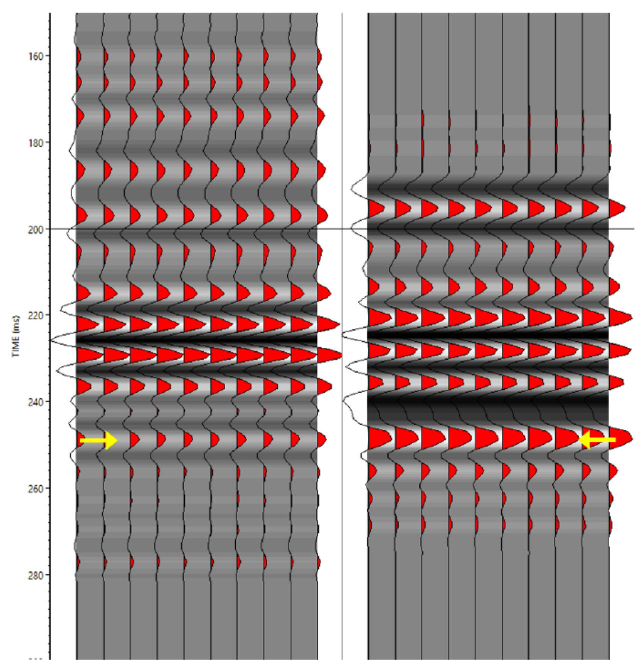


FIG. 4. Comparison of corridor stacks from VSP data acquired using GPUSA borehole linear vibrator sweep (left) and Vibroseis sweep (right), from Spackman and Lawton (2018).

## SEISMIC CONTINUOUS DATA

The previous section described the active seismic methods used at the Field Research Station. Each on the methods have their pro and cons.

1. The "conventional" active seismic surface is a known and widely used method for time-lapse studies (Landrø (2010) for example), but it can be heavy to repeat.

2. The Vertical Seismic Profiles, especially using DAS, allows a full vertical coverage but the uncertainty on the location and the depth channel still requires some work (Hall and Lawton, 2019). The low signal to noise ratio compared to the geophones is handled by the development of new fibers or interrogator units.

3. The permanently installed seismic sources allows a good repeatability of the measurements as these sources (and some receivers at the FRS) are fixed. It still remains a new technology and its use still requires some exploration.

Overall, the previously mentioned technologies remain punctual and can't capture the transient changes that we expect at the FRS. Innanen et al. (2019) propose to study the shift in amplitude and change of frequency content of seismic traces acquired during injection. This method still required active shots and can't be used continuously.

Acquisition of continuous seismic data is common in $CO_2$ storage monitoring, as well as hydraulic fracturing or EOR. It allows the induced seismicity study which is crucial for ensure the safety of $CO_2$ storage (but also hydraulic fracturing, EOR...). At the Field Research stations, we have 7 broadband stations that recorded continuously over the last 4 years as well as $\approx$ 6 months of data on denser and temporary experiments. Table 3 and Figure 5 describe the different surveys deployed at the Field Research Station.

| Survey Name | Broadband | Oct. 2017 | Feb. 2018 | Oct. 2018 | June 2019 | Cont. geophones |
|---|---|---|---|---|---|---|
| Recording duration | Since Oct. 2014 | 14days | 25 days | 7days | 25 days | since June 2019 |
| Instruments type | Broadband | geophones | geophones | geophones | geophones | geophones |
| Instruments number | 7 | 98 | 201 | 10 | 231 | 24 |
| Min. aperture | 250m | 10m | 10m | 10m | 20m | 43m |
| Max. aperture | 2.6km | 127m | 1.1km | 43m | 1.27km | 1.27km |
| Map on Fig 5 | a | b | c | d | e | f |

Table 3. Variation in elastic parameters.

Storke et al. (2018) and Gilbert et al. (2019) are focusing on the induced seismicity detection using respectively the STA/LTA method (Withers et al. (1998) per example) on broadband stations and the FAST (Bergen et al., 2018) method on geophones. In the present paper, we are studying the possibility to use the ambient noise correlation method for $CO_2$ injection and storage monitoring.

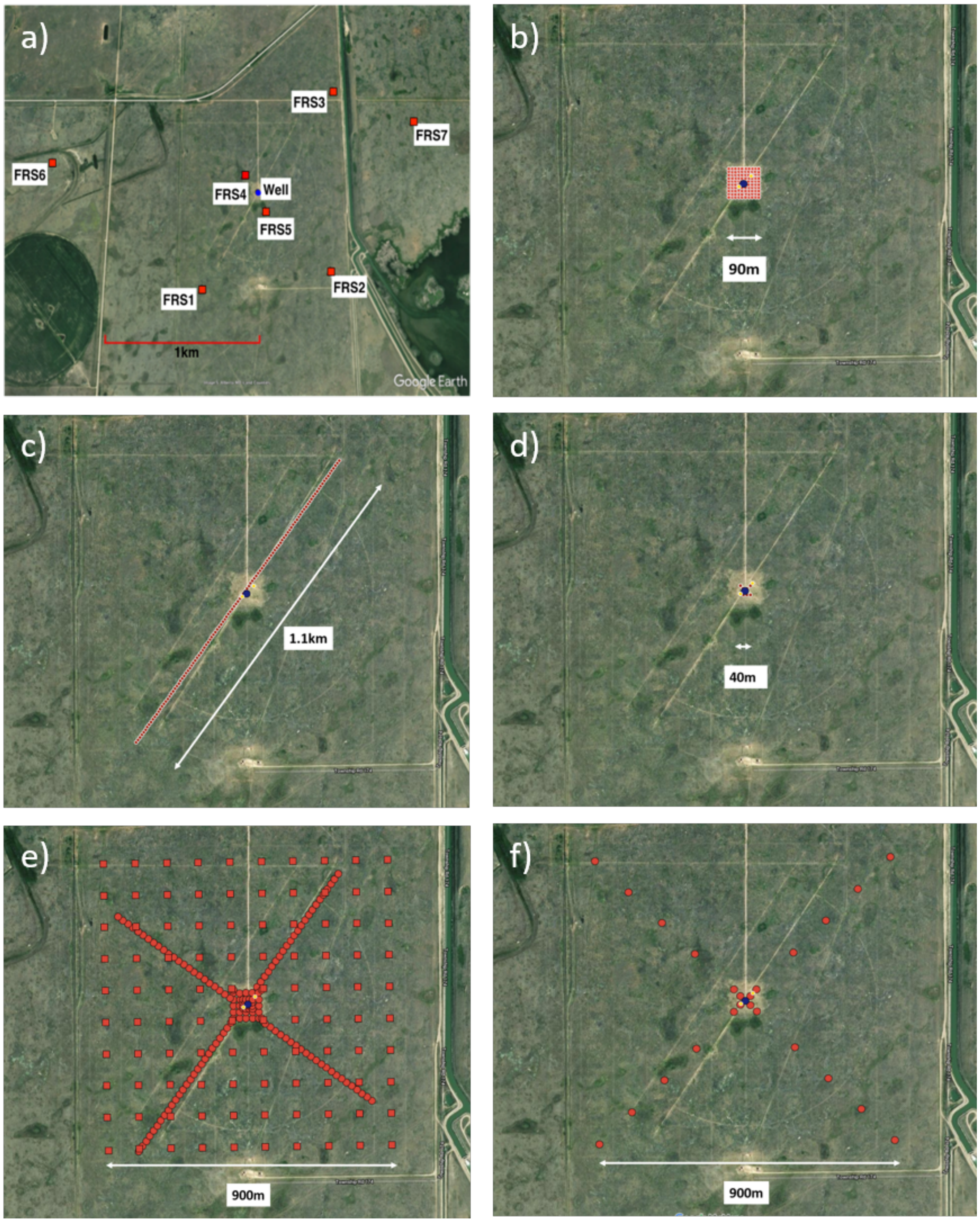


FIG. 5. Different configuration of surveys for continuous seismic data acquisition. Main parameters for each survey are described on Table 3. a) Broadband permanent stations; b) October 2017; c)February 2018; d) October 2018; e) June 2019 and f) since June 2019. Blue dot is the injection well, orange dots are the two monitoring wells.

## AMBIENT NOISE CORRELATION METHOD

### Theory

The majority of continuous seismic noise is composed by the ambient noise. It is generated by different phenomenon depending of the frequency:

- High frequencies (> $1Hz$) are due to anthropic noise such as roads, factories...
- $\approx Hz$ is due to local meteorological events such as rain or wind.
- High frequencies (< $1Hz$) are due to global meteorological events and oceans.

The seismic ambient noise method (sometimes called AN, or ANT for Ambient Noise Tomography) is based on the fact that you can approximate the Green's function between two receivers by correlating the continuous signal recorded at these two stations (Figure 6). In other words, you can turn one receiver into a so-called virtual source by correlating the ambient noise. In theory, we can recover the Green's function (impulsive response of the medium); in practice, only an approximation is reconstructed (due to non-homogeneous source of noise, attenuation...). The first applications on real data (Campillo and Paul (2003) and Shapiro and Campillo (2004)) were a huge step forward in crustal seismology. Indeed, the tomography of the crust was mainly possible using earthquakes. Seismic events are mainly localized along the active zones between tectonic plaques and are poorly repeatable. Be able to turn any receiver into a virtual source overpass that problem as well as the complex signature of seismic sources. Surface waves are dominant in the reconstructed Green's function, so the dispersion curves can be computed, group or phase velocity maps produced, then inverted to obtain V$_S$ model.

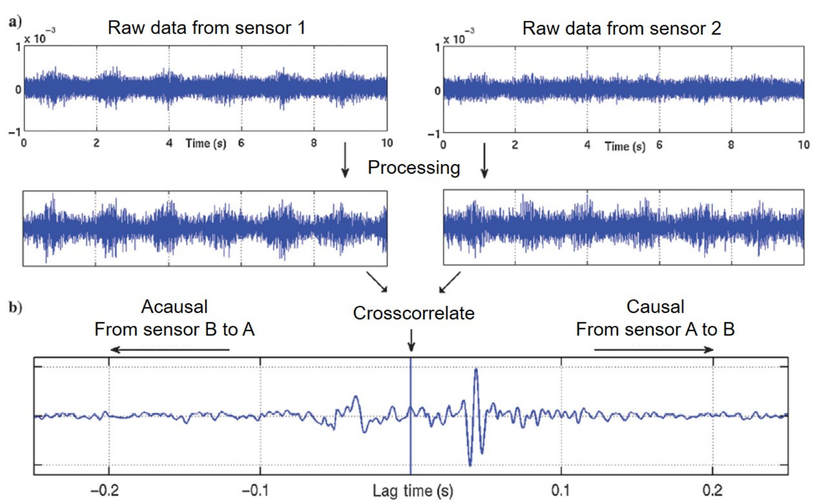


FIG. 6. Green's function reconstruction using ambient noise correlation method, modified from Olivier and Brenguier (2016).a) Raw and processed seismic signal for two sensors. b) Cross correlation results.

Over the past 15 years, a tremendous number of papers appears using this method, going from simple group (or phase) velocity maps to inverted V$_S$ tomography. The last step is not always done, and a lot of studies stop at the group or phase velocity stage. Indeed, the inversion from dispersion curve to $V_S$ model can be complex. The improvement of processing can now allow the emergence of body waves. In addition to tomography studies, the use of ambient noise correlation technique starts to be used for monitoring purposes. As the Green's function is sampling the medium between 2 stations, is the medium if changing (more or less scatters, change in velocities...), you should be able to use the correlations to track these changes (Fig. 7). Note that the coda of the Green's function is usually used as it is sampling the medium longer.

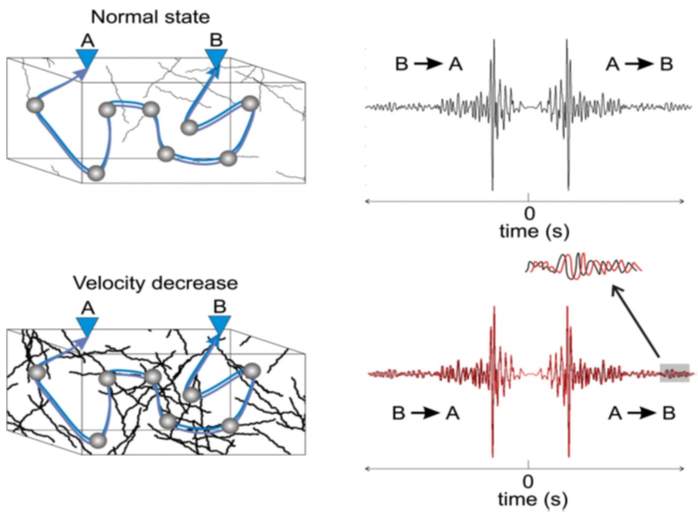


FIG. 7. Sketch representing the principle of seismic velocity change detection from travel time perturbations in the coda of noise correlation functions. Right: Corresponding correlation. In black, for the normal state, in red, with decreasing in the medium velocity, from Brenguier et al. (2016).

For the next part, we use MSNoise Python package for continuous seismic data processing and correlation computation (Lecocq et al., 2014).

## Processing

A careful processing needs to be applied to remove the effect of punctual events that can be observed in the continuous signal (regional earthquakes, local induced seismicity, vibe shot from active surveys, pump running during injection...). Indeed, those events are strongly correlated between stations and so may affect the results of the reconstructed Green's function.

The raw continuous signal is first downsampled from 1000 to 100Hz to reduce the computing time, the mean and trend are then removed. Temporal and spectral normalization are applied. We use the 1bit method for the first one, which consist of putting to -1 all the negative amplitudes and to +1 all the positive amplitudes. We use the spectral whitening as spectral normalization. This method flattens the frequency content and boost the lack of certain frequencies and lower the dominant ones.

Figure 8.a and b shows an illustration of the processing on 30 seconds of noise. Spectrogram of the raw signal already shows a nice flat spectrum over time. 1bit processing is illustrated on Figure 8.a, middle row. We can notice that this temporal processing may act

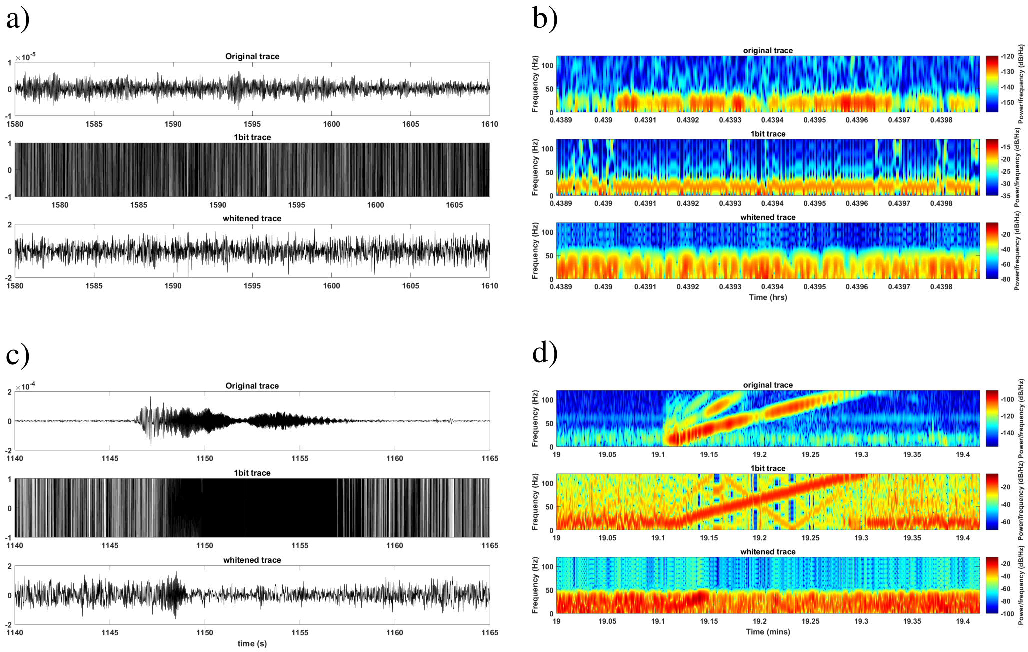


FIG. 8. a) 20s of noise, top: raw trace. Middle: 1bit processing. Bottom: Spectral whitening. b) Corresponding spectrogram. d) Corresponding spectrogram. c) 25s of Vibe signal, top: raw trace. Middle: 1bit processing. Bottom: Spectral whitening. d) Corresponding spectrogram.

like as filer at some high frequencies are sometimes introduced (for example at 0.4397 on Figure 8.b, middle row). Last step of the processing, the spectral whitening (here between 1-50Hz for illustration) re-flatten the spectra of the signal (Figure 8.b, bottom row).

Figure 8.c and d shows the effects of the processing on 30s of signal containing one shot of vibe. As explained in previous section, we clearly see the effect of the vibe shot on the raw spectrogram (Fig. 8.d, top row). 1bit processing (middle rows) clearly reduces the high amplitudes due to the shot. However, the spectrogram (Fig. 8.d middle row) still clearly shows the high frequencies content due to the shot (also observed on the signal on Figure 8.c, middle row). Spectral whitening erases the high frequencies and flattened the spectrum as shown on Figure 8.d, bottom row.

## Green's function reconstruction

We correlated the daily correlation for all the pairs of stations. The daily correlations are stacked to obtain the reference correlation.

Figure 9 shows a reconstructed shot gather. It represents the correlation between one station (yellow star) and all the other stations. The yellow station is turned into a virtual source. We stack the causal and acausal part. We can see the surface wave (here Rayleigh wave as we use the vertical components)with a velocity of $\approx 325 km.s{-}1$. We interpret the faster wave as a body wave. We compute the cross correlation between all the pairs of stations, and obtain a starting dataset of 4098 paths for the next steps.

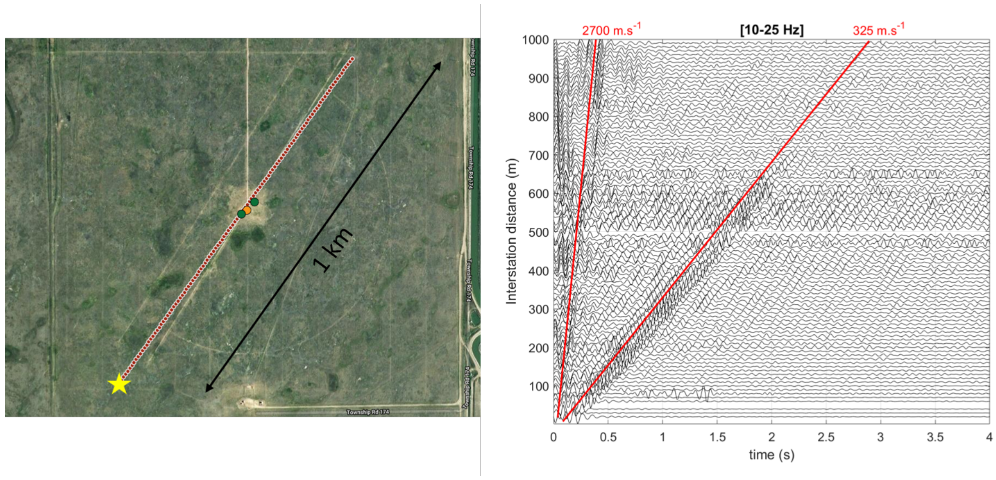


FIG. 9. Virtual shot gather reconstructed with the Ambient noise correlation method. Left: experiment layout, yellow star is the receiver turned into a virtual shot. Orange dot is the injection well, green dots are the observation wells. Right is the reconstructed shot gather.

## Application to near surface tomography

Some studies are done at the Field Research Station to characterize the near surface. This characterization is crucial for the processing of active seismic data, especially for time-lapse study with small expected variations. The previous studies will help to validate the model obtain using the correlation method.

The surface waves are dominant in the reconstructed Green's function. Surface waves are dispersive, we can compute the group and phase velocities for each period, giving us the dispersion curve. The dispersion curves (here group velocity) between each pair of stations can be regionalized to obtain local dispersion curves in each grid point. These dispersion curves can be inverted to obtain local 1D-elastic parameters models. The combination of the 1D models give a pseudo 2D model.

### *Dispersion curves*

We sum the causal and acausal part of the correlation and use the frequency-time analysis method (FTAN, Levshin et al. (1989)) to compute the group velocity dispersion curves between each pair of stations. The correlations are first quality-controlled and we remove s portion of the whole dataset. It is based on:

- The signal to noise ratio (SNR) criteria, i.e. the quality of the reconstructed Green's function. The histogram of the SNR is shown on Figure 10.a. We choose to keep the correlation with a SNR higher than 5. We remove close to 1000 of the "worst" correlations (Figure 10.c).
- The $\lambda$ criteria, i.e we want to keep only the path containing at least one wavelength (Luo et al., 2015). Figure 10.c shows the number of paths after applying this criteria (in addition to the previous one). We can see that we remove more paths at low frequencies ($\lambda$ is larger than at high frequencies).

- Removing the outliers measurements. We test this step by keeping only the group velocity $\pm$ 0.1km.s$^{-1}$ the mode velocity (Figure 10.b. Because of the large number of values and the Gaussian distribution of the velocities, removing the outliers does not really change the results. Rather than choosing an arbitrary threshold value, we choose to keep all the velocities.

The final number of correlations used in the following step is shown by the yellow curve on the Figure 10.c. Figure 11 shows the probability density function of the dispersion curves kept for next step. Red curve is the theoretical dispersion curves computed from well logs and near surface analysis (Isaac and Lawton (2019)).

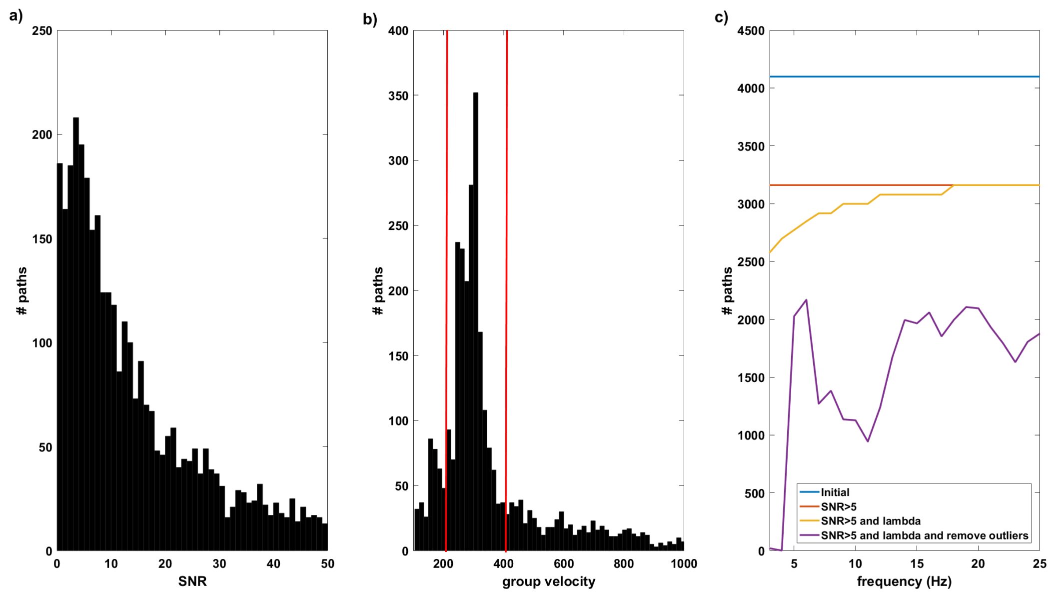


FIG. 10. a) SNR distribution. b) Group velocity distribution. Red lines represents the mode velocity $\pm$ 100m.s$^{-1}$. c) Number of correlations keep as a function of the QC criteria.

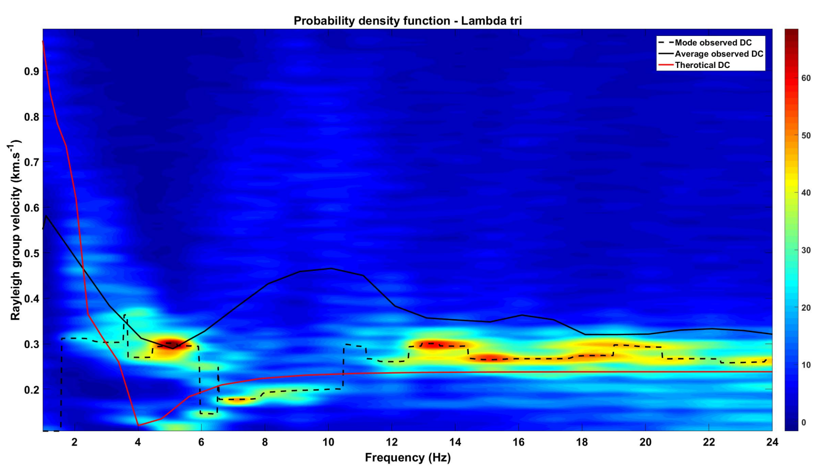


FIG. 11. Probability density function of the dispersion curves after application of the SNR and lambda criteria.

*Group velocity map and 2D group velocity model*

We regionalize the dispersion curves computed between each pair of stations using the method of Barmin et al. (2001). We here present a brief summary of the method and refer the reader to Mordret et al. (2013) for detailed discussion. The model $m$ is estimated by minimizing the penalty function :

$$S(m) = (G_m - d)^T C_d^{-1}(G_m - d) + m^T G_m \tag{1}$$

where $d$ is the data vector, $G$ is the forward operator, $C_d$ is the data covariance and $Q$ is the regularization matrix. The regularization matrix is based on the lateral smoothing and the damping which are determined using L-curves. The cell size is 10m large, and the number of paths in the middle of the model can reach up to 1000. We produce a 1D group velocity model following the trench for each frequency (Figure 12).

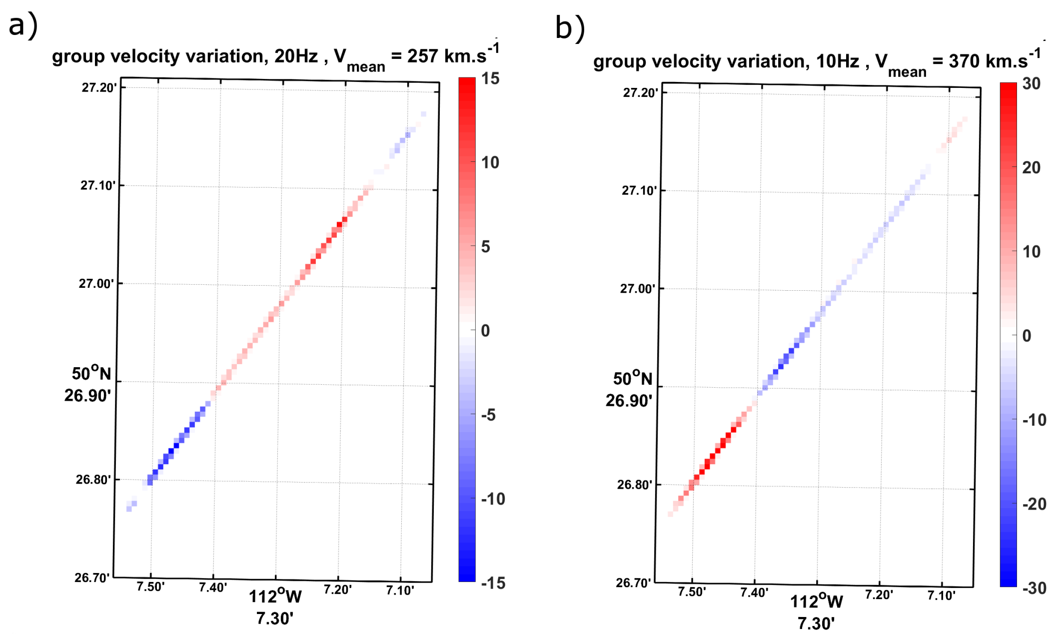


FIG. 12. Group velocity variation along the trench. a) At 20Hz. b) At 10Hz. The mean group velocity is indicated on the top of the map. 20Hz is sensitive to shallower part than 10Hz.

The 1D maps are combine to obtained the 2D group velocity presented in Figure 13. They are expressed in variation as function of the averaged group velocity. It is difficult to directly compare group velocities and S-wave velocities as the relation between group velocity and S-wave velocity is not linear. V$_g$ is mainly dependent of V$_S$ but also depends the density, V$_P$, the attenuation... Nevertheless, the following considerations are true:

1. Low group velocity can be related to low S-wave velocity.
2. High frequencies are sensitive to shallow part when lower frequencies are sensitive to deeper part.

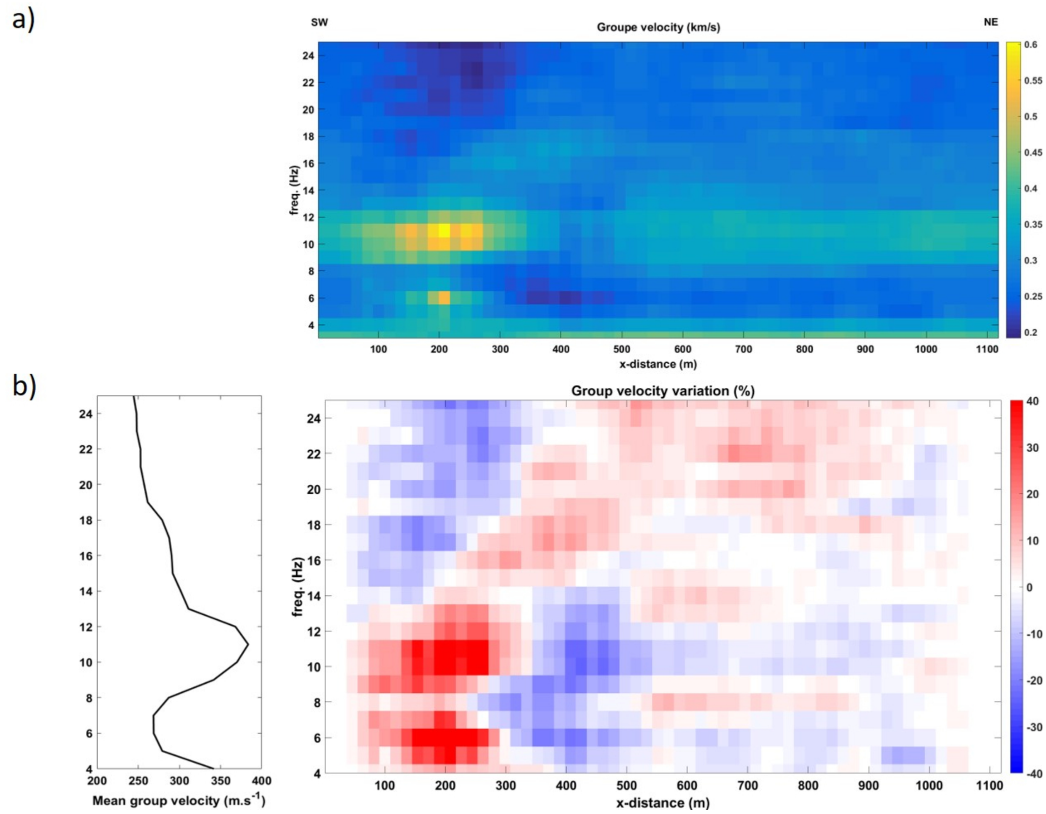


FIG. 13. a) Group velocity section along the trench. b) Group velocity variation (left) compared to mean velocity at the specific period (right).

From these considerations, we can observe on Figure 13 that:

- the velocities are increasing with depth;
- *at shallow depth*: velocity is lower on the SW part than on the NE part of the trench;
- *at deeper depth*: velocity is higher on the SW part than on the NE part on the trench.

These observations are coherent with the results of Isaac and Lawton (2019).

### *Local dispersion curve inversion*

We extract the local dispersion curve for each cell of the 2D model and invert it to get the local V$_S$ model for that location. We use srfpython package developed by Lehujeur et al. (2018). It computes and inverts surface wave dispersion curves (Rayleig and/or Love, phase and/or group velocity, fundamental and/or higher modes...), and is based forward modelling computation of Herrmann (Computer Program in Seismology, Herrmann (2013). The Herrmann's codes give also the possibility to invert dispersion curves, but it is based on a linearized inversion. Lehujeur et al. (2018) implement the Monte Carlo approach in their codes. Using Monte Carlo algorithm allows a better exploration of the model space and avoid the risk to be trapped in local minima that can happen using linearized inversion.

We use the boundaries presented in table 4 for the models space exploration. It is based on the velocity model in Isaac and Lawton (2019) but we keep wide boundaries in order to not constrain to much the inversion and allow a higher degree of freedom for the inversion.

| Layer Number | Top depth range (m) | Vs range ($m.s^{-1}$) |
|---|---|---|
| 1 | 0 | 100 - 300 |
| 2 | 0.5 - 10 | 100 - 300 |
| 3 | 20 - 40 | 600 - 2000 |

Table 4. Prior boundaries of uniform probability distribution used.

12 independent Morkov chains are running in parallel until 500 models are retained and we keep 2500 best models of the 6000 selected ones. Figure 14 shows the results for one dispersion curve. Left are the retained model, color plotted as a function of their likelihood and right are their associated dispersion curve. The final model is the average of the 2500 best ones (grey curve).

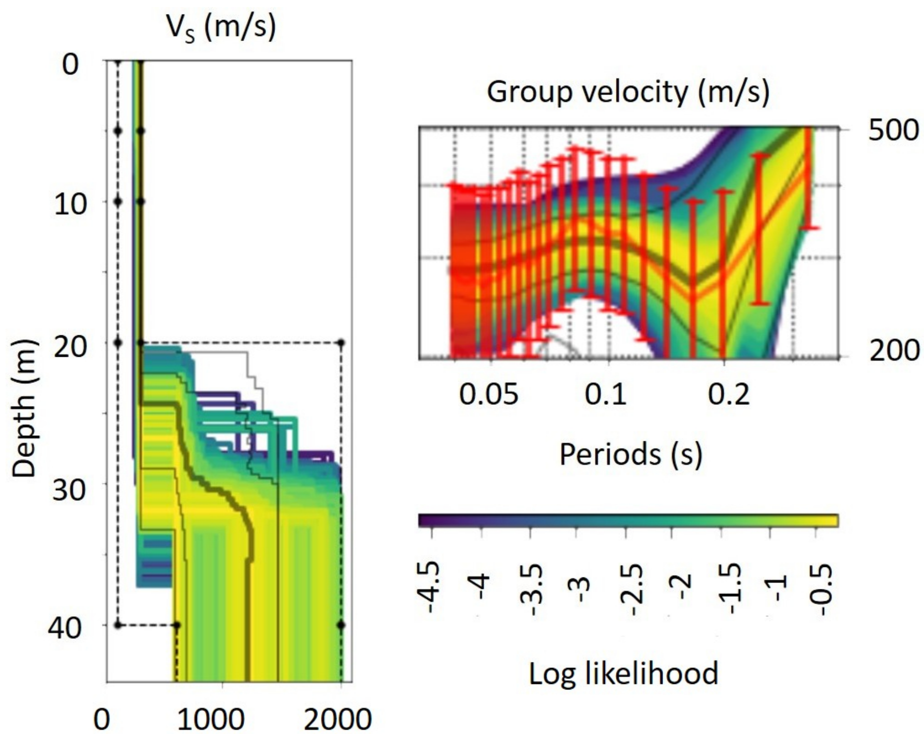


FIG. 14. Inversion of a local dispersion curve. Right: 2500 best models. Dotted black lines is the explored model space described in Table 4. Grey is the final model. Left: associated dispersion curves. Red is the observed one, with associated errors.

*2D Vs model*

We run the inversion describe in the previous subsection for each local dispersion curves and we combine the S-wave models obtained to get the 2D section.

Isaac and Lawton (2019) and Qu et al. (2019) produce near surface $V_S$ models for the CaMI.FRS. Isaac and Lawton (2019) use data from a shear source and obtain a 2D model along the trench. Qu et al. (2019) used data from a low-frequency Vibroseis truck on DAS

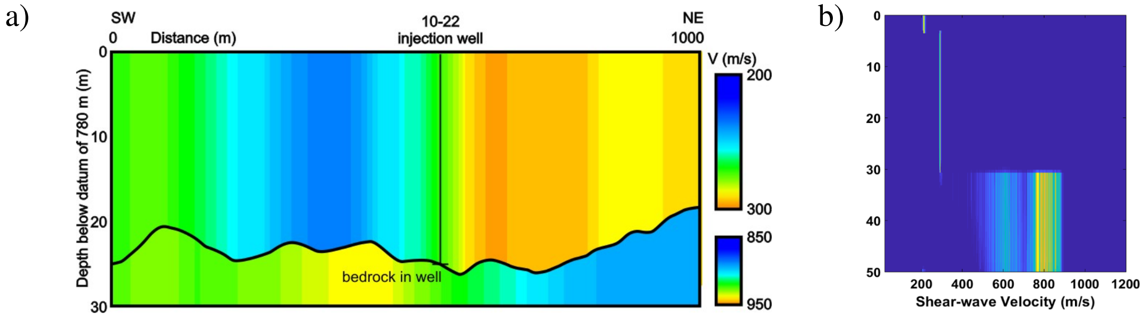


FIG. 15. S wave velocity model from other study. a) From Isaac and Lawton (2019). b) From Qu et al. (2019).

data along the trench. Because they use active sources, the quality of the data differs from the data of the present study. Isaac and Lawton (2019) clearly see the first breaks as well as a refractor in their data. By picking first breaks and doing refraction static analysis, they obtain a 2-layers 2D model with bedrock depth (Figure 15.a).

Qu et al. (2019) are able to pick higher mode which remain difficult using ambient noise correlation method. They are able to better constrain the inversion process by using those higher modes. On the other hand, they obtain an average 1D $V_S$ model rather than a 2D model (Figure 15.b).

Figure 16 is the result of the inversion using ambient noise correlation process. Due to the chosen inversion method (average of the best 2500 models found using Monte Carlo inversion), there is no clear interface in our model but more a "interface" gradient. Nevertheless, our $V_S$ model is consistent with other studies.

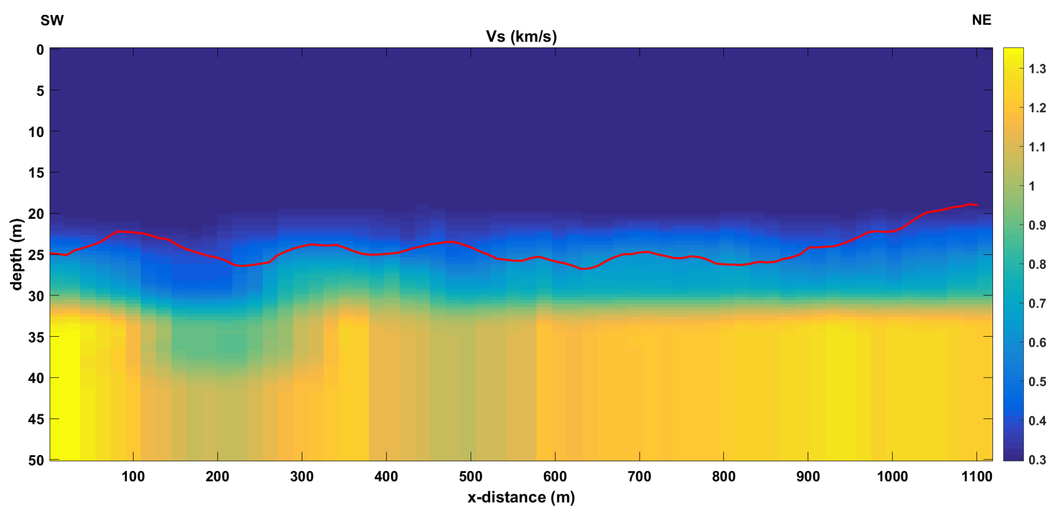


FIG. 16. Inverted $V_S$ model along the trench. Red line is the bedrock depth obtained from shear wave source analyses (Isaac and Lawton, 2019).

## Application to monitoring

As mentioned before, the reconstructed Green's function can be used to track the changes of the medium.

Several studies are exploring the use of the ambient noise correlation to study the velocity changes and are positively concluding. Several studies are focusing on volcanoes (Duputel et al., 2009; Lecocq et al., 2014; Brenguier et al., 2016; Olivier et al., 2019), geothermal site (Obermann et al., 2015), reservoir injection stimulation (Hillers et al., 2015a), landslide (Mainsant et al., 2012) or even dam integrity (de Wit and Olivier, 2018).

The quantification and the interpretation of the velocity changes remains difficult as the relation between changes and strain is complex and not yet perfectly established. Several papers study the correlation between the source of noise and the environmental parameters. Studying the noise amplitude and the H/V ratio, Hillers and Ben-Zion (2011) show link between wind, temperature and noise amplitudes for frequencies higher to 1Hz. Hillers et al. (2015b) study the velocity variations in the noise correlation between 0.5 and 2Hz. They associated the observed velocity variation of $\approx 2\%$ to the thermoelastic strain induces by atmospheric temperature variations. Other environmental effects such as wind, rainfall, ground water level and barometric pressure may also produce secondary variations. Meier et al. (2010) attribute the $0.1\%$ velocity variations they are observing in the ambient noise correlation to ground-water aquifer level change and thermo-elastic strain. Mao et al. (2019) are showing the link between the velocity variation and the tides and solar radiations.

The previous cited studies shoes that the influence of environmental changes such as temperatures can play a huge role and induce velocity variation that can be high (up to $2\%$ in Hillers et al. (2015b)). Understand the impact of the environmental changes is crucial if we want to use the ambient noise correlation for monitoring, especially we expect small velocity changes, such as at the Field Research Station. In our case, the changes expected due to $CO_2$ are relatively small, not so much by the elastic parameters variation but by the size of the affected zone. The expected elastic parameters variation can be quite high especially by taking account the pressure effect (up to -20% for $V_S$, Figure 2) but the injection simulation gave a plume size of $\approx$200m horizontally and $\approx$15m vertically (Macquet et al., 2019).

To understand the impact of environmental changes such, we use the broadband stations array (Figure 5.a) we have deployed at the Field Research Station since October 2015 Figure 17).

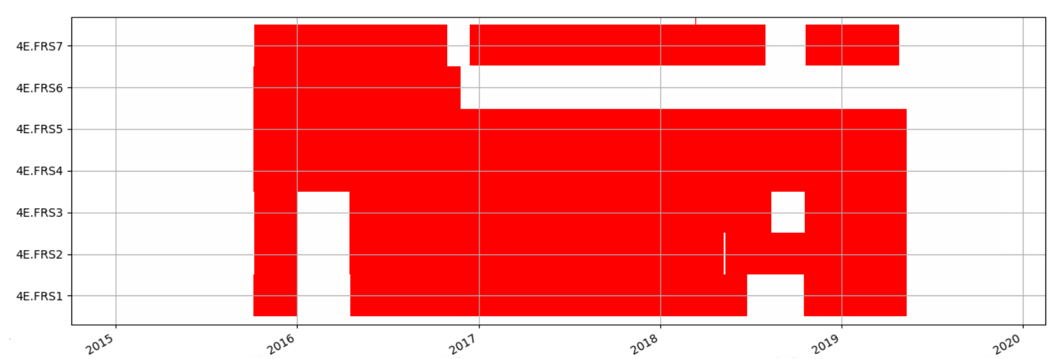


FIG. 17. Data availability for the 7 broadband stations. For their location, refer to Figure 5.a. FRS6 had GPS trouble from October 2016 to May 2019 (last data harvest).

Figure 18 shows the daily correlation between FRS4 and FRS5, processed between 0.1 and 40Hz. We can clearly see a seasonal pattern, with slower arrival during winter periods than summer periods. Figure 19 show the daily correlation but filtered between 0.1 and 1 Hz on Fig. 19.a and between 1 and 10 Hz on Fig. 19.b. We can observe that the seasonal variations (winter/summer) are clearly visible on Figure 19.a but disappears on 19.b.

Note that we display the correlation between FRS4 and FRS5 because it is the only pair of stations that is covering the whole period, but the observations are the same for the other pairs of stations.

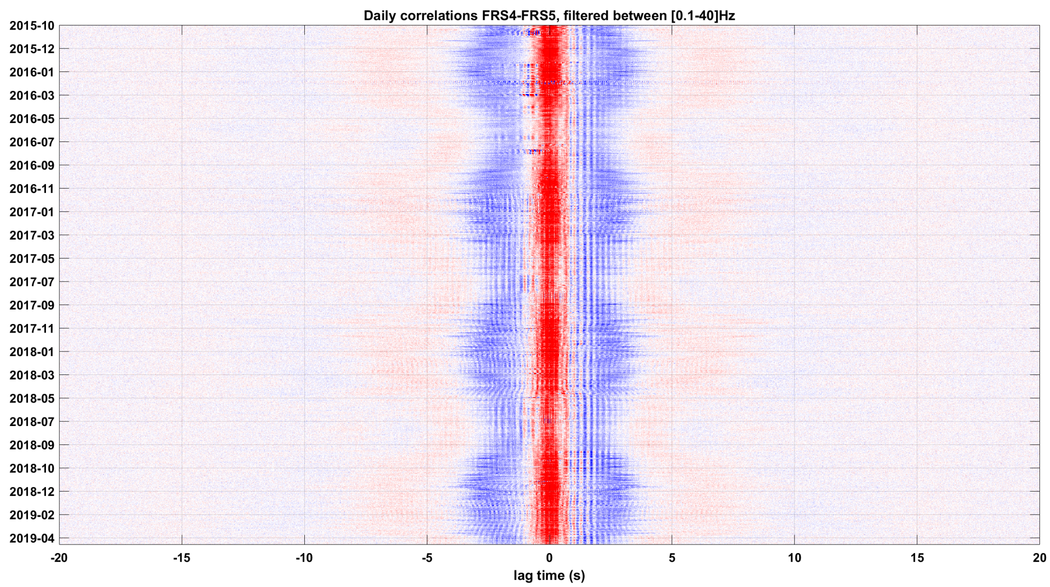


FIG. 18. 4 years of daily correlations between two broadband stations (FRS4 and FRS5).

a) b)

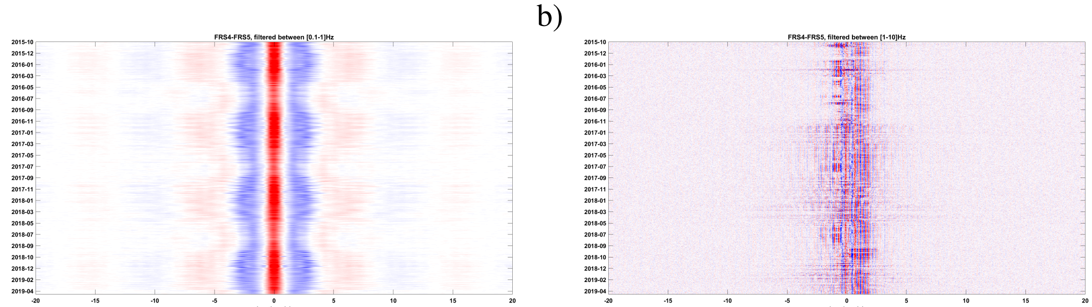


FIG. 19. Daily correlation between FRS4 and FRS5 (for location see Figure 5.a. a) Filtered between 0.1 and 1Hz. b) Filtered between 1 and 10Hz.

Two main methods are used to quantify the velocity variations observed in the correlation of ambient noise (Obermann, 2013): the stretching method and the Moving-Window Cross Spectrum analysis. They compared a reference correlation (usually the stacked of all the daily correlations) and a current correlation (daily or n-days stacked correlation). In the MSNoise package, Lecocq et al. (2014) implement the Moving-Window Cross Spectrum analysis (MWCS, first introduced by Ratdomopurbo and Poupinet (1995), also called doublet method). Figure 20 describes the principle (Obermann, 2013). For a detailed theory, lectors can refer to Clarke et al. (2011).

Three parameters will influence the results if the Moving-Window Cross Spectrum analysis:

- The filtering of the correlation.
- The number of daily correlations used to produce the current correlation.
- The correlation time windows used to compute the $\delta v/v$. The direct waves observed in the ambient noise correlation are more sensitive to the directional changes in the noise distribution than the seismic coda, which is multiply scattered waves (Colombi et al., 2014; Hadziioannou et al., 2009). The longer the waves travels through the medium (i.e late coda), the more sensitive they are to in-situ velocity variation.

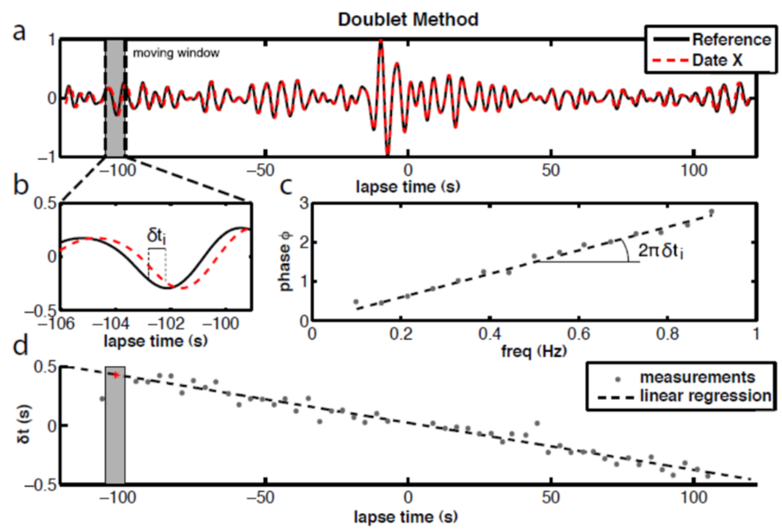


FIG. 20. Doublet method principle, from Obermann (2013). a) Reference signal reference correlation (black) and time delayed signal current correlation (red). b) Zoom into the windowed cross-correlations functions, marked with the shaded grey area in Fig. 20.a. c) The phase of the cross-spectrum of the windowed cross-correlations. The slope is equal to $2\pi\delta t$. d) Estimation of $\delta t/t$ via linear regression of the delay measurements in all time windows. $\delta v/v$ is then estimated as - $\delta t/t$

Figure 21 some of the parameters that can produce changes of the subsurface and so induces velocity changes. To compare the velocity changes observed in the correlation and the parameters displayed on Figure 21, we compute the correlation coefficient between the two curves: if the correlation coefficient is equal to 1 then the two curves are perfectly correlated; if the correlation coefficient is equal to -1 then the two curves are perfectly anti-correlated; if the correlation coefficient is equal to -1 then there is no relationship between the two variables.

Figure 22 shows the average velocity variation observed for all pairs of stations. The analysis is done in the [0.1-1]Hz frequency range. Figure 22.a shoes the daily velocity variation as well as the curves (over 40 days). We can clearly see a good correlation between the smoothed curve and the average temperature (Figure 22.b). Figure 22.c shows the daily $CO_2$ injection, with the periods of injection highlighted in green. They seem to correspond to periods of velocity variation decreasing (Figure 22.a).

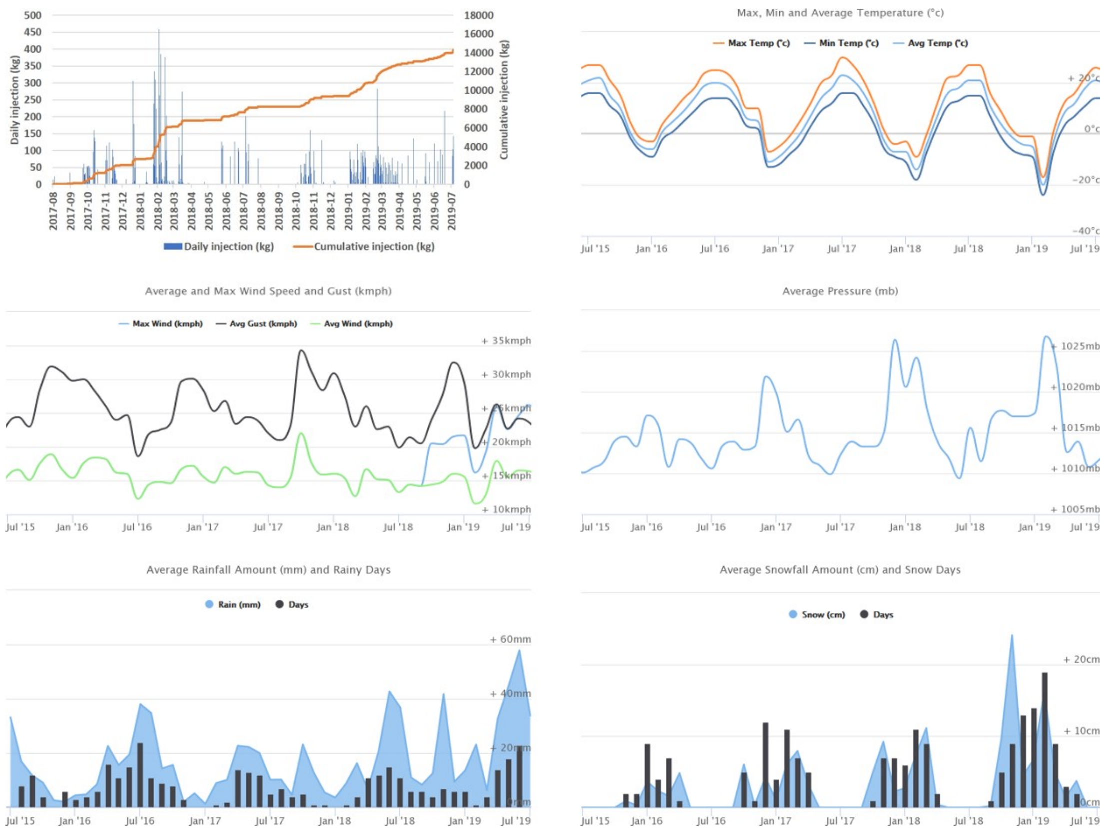


FIG. 21. $CO_2$ injection at the Field Research Station. Environmental parameters (temperature, wind, pressure, rain fall and snow fall) at Brooks (From http://agriculture.alberta.ca/acis/alberta-weather-data-viewer.jsp). Note that the time scale for the $CO_2$ injection is only going from July 2017 to July 2019.

The analysis of the velocity variation clearly shows the influence of the temperature. It seems that other parameters such as precipitations and $CO_2$ injection. A deeper work is required to confirm the first observations. It includes:

- an analysis of velocity variation observed for each individual pairs of stations and not only the average of them, and maybe find a geographical pattern for the velocity changes which can be linked to $CO_2$ injection for example;
- an analysis of the different filters and their impact on the observed velocity changes;
- an analysis of the different number of days stacked (for example the temperature effect has a long period effect compare to the injection effect or the wind);
- an analysis of the different windows of $\delta v/v$ computation, i.e. early or late coda.

We also need to compare the velocity variations with other parameters such as tidal model, reservoir pressure, atmospheric pressure and understand the link between all those parameters and the velocity variation. A comprehensive analysis of the causes of the observed velocity variation is crucial if we want to be able to associate possible $CO_2$ injection to velocity variation.

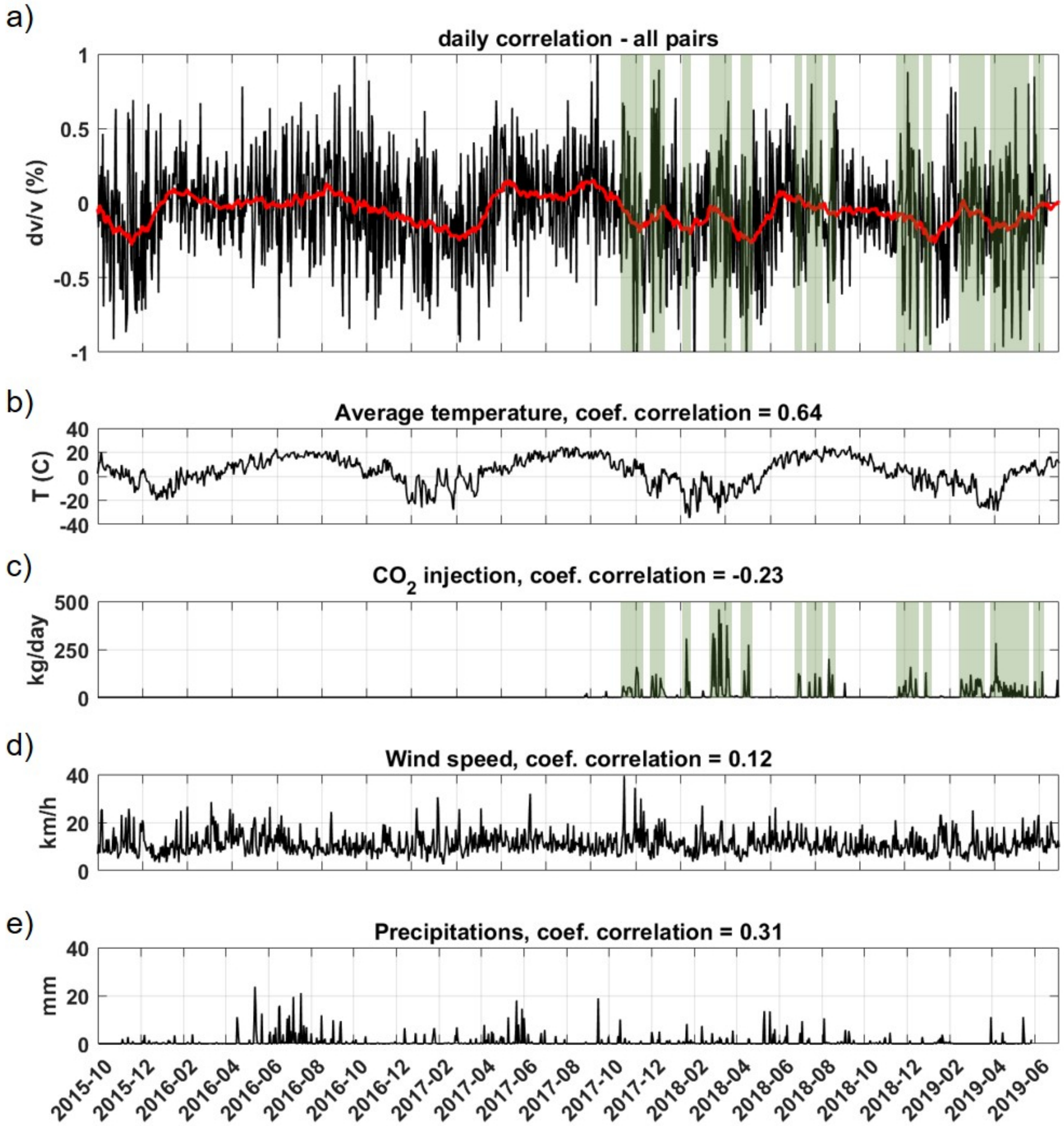


FIG. 22. a) Velocity variation from daily cross correlation. Red curve is the smoothed curve. b) Average daily temperature. c) Daily injection. d) Wind speed at 2m high. e) Rain precipitation.

## FUTURE WORK

The near surface tomography work can be extended to the June 2019 survey. The 3D part of that experiment will be used to have a 3D Vs model of the subsurface. The trench part of that experiment will be used to compare the velocity obtained during winter time (Feb. 2018, this study ) and summer time (June 2019, future work) and determine the effect that the environmental changes can have on the near surface conditions.

The monitoring work will be updated with the continuous acquisition on the broadband array. Since June 2019, seismic continuous acquisition was also done on 24 geophones. During that period, the $CO_2$ injection increases. Monitoring trough ambient noise correlation and trough events detection will be carrying on.

In general, general working continuous seismic data give a lot of opportunities such as:

- Beamforming to better understand the noise field at the Field Research Station. The 3D June 2019 survey (Figure 5.e) is a good candidate for that study.
- $H/V$ ratio.
- Love waves.
- Joint inversion with other methods, such as the phase velocity observed on the DAS (Qu et al., 2019) or the receiver function (Gilbert et al., 2019).

## CONCLUSIONS

Concerning the imaging of subsurface with ambient noise; the method is already widely attested, in particular among the crustal tomography field. The downside part in this study is the shallow depth of investigation due to the frequency range of the used geophone. However, the $V_S$ model is coherent with other studies done at the Field Research Station.

Concerning the monitoring of $CO_2$ injection with the ambient noise correlation method, the main challenge at the Field Research Station is the weak amount of $CO_2$ that is planned to be injected in order to simulate a leakage. 500kg/day will induce relatively small plume size (compare to large-scale field) and small variation in elastic parameters. As the use of ambient noise can highly be affected by environmental changes, a very careful analysis of the system is required to fully understand which parameters influences the Green's function reconstruction and so which parameters can be the cause of the velocity variation observations. The 4 years of continuous recording on the broadband stations and several weeks on several denser surveys allow the study of the impact of the environmental changes on the ambient noise correlation method. The effect of the seasonal temperature is clearly visible on the velocity variation curves. We also suspect an effect of the $CO_2$ injection. Further analysis is required to confirm the first observations and be able to associate observed velocity variation to the correct parameters. Ultimate goal being to determine if whether or not the ambient noise correlation technique can be used to detect leakage of $CO_2$.

## ACKNOWLEDGEMENTS

We thank CaMI JIP and CREWES sponsors for continued support. We also gratefully acknowledge support from NSERC (Natural Science and Engineering Research Council of Canada) through the grant CRDPJ 461179-13. This research was undertaken thanks in part to funding from the Canada First Research Excellence Fund. We thank Anna Storke and Rob Kendall for access to the broadband data. We thank Thomas Lecocq for developing and distributing the MSNoise codes.

## REFERENCES

Arts, R., Chadwick, A., Eiken, O., Thibeau, S., and Nooner, S., 2008, Ten years' experience of monitoring $CO_2$ injection in the Utsira Sand at Sleipner, offshore Norway: First break special topic $CO_2$ sequestration, **26**.

Barmin, M. P., Ritzwoller, M. H., and Levshin, A. L., 2001, A fast and reliablemethod for surface wave tomography: Pure App. Geophys., 1351–1375.

Bergen, K., Yoon, C. E., Rong, K., Bailis, P., and Beroza, G. C., 2018, Fast: a data mining approach to large-scale earthquake detection, *in* AGU Fall Meeting Abstracts.

Bergmann, P., Ivandic, M., Norden, B., Rücker, C., Kiessling, D., S., S. L., Schmidt-Hattenberger, C., and Juhlin, C., 2013, Combination of seismic reflection and constrained resistivity inversion with an application to 4d imaging of the $CO_2$ storage site, Ketzin, Germany: Geophysics, **79**, No. 2, B37–B50.

Bouchedda, A., and Giroux, B., 2016, Mmr measurements at the field research station, alberta, 2016: CAMI Research Report, **1**.

Brenguier, F., Rivet, D., Obermann, A., Nakata, N., Boué, P., Lecocq, T., Campillo, M., and Shapiro, N., 2016, 4-d noise-based seismology at volcanoes: Ongoing efforts and perspectives: Journal of Volcanology and Geothermal Research, **321**, 182–195.

Campillo, M., and Paul, A., 2003, Long-range correlations in the diffuse seismic coda: Science, **299**, No. 5606, 547–549.

Clarke, D., Zaccarelli, L., Shapiro, N., and Brenguier, F., 2011, Assessment of resolution and accuracy of the moving window cross spectral technique for monitoring crustal temporal variations using ambient seismic noise: Geophysical Journal International, **186**, No. 2, 867–882.

Colombi, A., Chaput, J., Brenguier, F., Hillers, G., Roux, P., and Campillo, M., 2014, On the temporal stability of the coda of ambient noise correlations: Comptes Rendus Geoscience, **346**, No. 11-12, 307–316.

de Wit, T., and Olivier, G., 2018, Imaging and monitoring tailings dam walls with ambient seismic noise: 21st International Seminar on Paste and Thickened Tailings.

Dongas, J. M., 2016, Development and characterization of a geostatic model for monitoring shallow $CO_2$ injection: Master Thesis, University of Calgary.

Duputel, Z., Ferrazzini, V., Brenguier, F., Shapiro, N., Campillo, M., and Nercessian, A., 2009, Real time monitoring of relative velocity changes using ambient seismic noise at the piton de la fournaise volcano (la Réunion) from january 2006 to june 2007: Journal of Volcanology and Geothermal Research, **184**, 164–173.

Gilbert, H., Savard, G., Gu, J., Macquet, M., and Lawton, D., 2019, Passive seismic monitoring at the cami field research staion, aberta, canada: Containment and Monitoring Institute and CMC Research Institutes Suscriber workshop.

Gordon, A., 2019, Processing of DAS and geophone VSP data from the CaMI Field Research Station: Master Thesis, University of Calgary.

Gordon, A., and Lawton, D. C., 2017, Zero offset VSP processing of fiber optic cable (DAS) and geophone array at the CaMI Field Research Station: CREWES Research Report, **29**.

Gordon, A., and Lawton, D. C., 2018, Walk away VSP processing of DAS and geophone data at the CaMI Field Research Station, Newell county, Alberta: CREWES Research Report, **30**.

Gordon, A., and Lawton, D. C., 2019, Walkaway VSP processing of DAS and geophone data at the CaMI Field: Containment and Monitoring Institute and CMC Research Institutes Suscriber workshop.

Gordon, A., Lawton, D. C., and Eaton, D. W., 2016, VSP azimuthal travel time analysis at the Field Research Station near Brooks, Alberta: CREWES Research Report, **28**.

Hadziioannou, C., Larose, E., Coutant, O., Roux, P., and Campillo, M., 2009, Stability of monitoring weak changes in multiply scattering media with ambient noise correlation: Laboratory experiments: The Journal of the Acoustical Society of America, **125**, No. 6, 3688–3695.

Hall, K. W., Bertram, K., Bertram, M., Innanen, K., and Lawton, D., 2018, Crewes 2018 multi-azimuth walk-away VSP field experiment: CREWES Research Report, **30**.

Hall, K. W., Isaac, J. H., Wong, J., Bertram, K. L., Bertram, M. B., Lawton, D. C., Bao, X., and Eaton, D., 2015, Initial 3C-2D surface seismic and walkaway VSP results from the 2015 Brooks SuperCable experiment: CREWES Research Report, **27**.

Hall, K. W., and Lawton, D., 2019, Assigning receiver locations to DAS traces at the CaMI.FRS: CREWES Research Report, **this volume**.

Hall, K. W., Lawton, D. C., Daley, T., Freifeld, B., and Cook, P., 2017, Source distance and source effort on DAS data: CREWES Research Report, **29**.

Herrmann, R. B., 2013, Computer programs in seismology: An evolving tool for instruction and research: Seismological Research Letters, **84**, No. 6, 1081–1088.

Hillers, G., and Ben-Zion, Y., 2011, Seasonal variations of observed noise amplitude at 2-18Hz in southern california: Geophysical Journal International, **184**, 860–868.

Hillers, G., Husen, S., Obermann, A., Planès, T., Larose, E., and Campillo, M., 2015a, Noise-based monitoring and imaging of aseismic transient deformation induced by the 2006 basel reservoir stimulation: Geophysics, **80**, No. 4, KS51–KS68.

Hillers, G., Husen, S., Obermann, A., Planès, T., Larose, E., and Campillo, M., 2015b, Noise-based monitoring and imaging of aseismic transient deformation induced by the 2006 basel reservoir stimulation: Geophysics, **80**, No. 4, KS51–KS68.

Innanen, K., Lawton, D. C., Hall, K. W., Bertram, M., and Bertram, K., 2019, Tiny bubbles: seeking transient seismic signatures associated with $CO_2$ injection: CREWES Research Report, **this volume**.

Isaac, J. H., and Lawton, D. C., 2015, 3D3C seismic data at the Brooks experimental $CO_2$ injection site: CREWES Research Report, **27**.

Isaac, J. H., and Lawton, D. C., 2017, A summary of surface seismic reflection data acquired at the field research station near brooks, alberta: CREWES Research Report, **29**.

Isaac, J. H., and Lawton, D. C., 2019, Near-surface depth/velocity models at the CaMI Field Station: CREWES Research Report, **this volume**.

Landrø, M., 2010, 4d seismic, *in* Petroleum Geoscience, Springer, 489–514.

Lawton, D. C., Bertram, M., Bertram, K., Hall, K., and Isaac, H., 2015a, A 3C-3D seismic survey at a new field research station near Brooks, Alberta: CREWES Research Report, **27**.

Lawton, D. C., Bertram, M., and Bertram, K. H. K., 2015b, New approaches to seismic monitoring at the Brooks Field Research Station: CREWES Research Report, **27**.

Lecocq, T., Caudron, C., and Brenguier, F., 2014, MSNoise, a Python package for monitoring seismic velocity changes using ambient seismic noise: Seismological Research Letters, **85**, No. 3, 715–726.

Lehujeur, T., Vergne, J., Schmittbuhl, J., Wigone, D., Le Chenadec, A., and EstOF Team, 2018, Reservoir imaging using ambient noise correlation from a dense seismic network: Journal of Geophysical Research-Solid Earth, **123**, No. 8, 6671–6686.

Levshin, A., Yanocskaya, T. B., Lander, A. V., Bukchin, B. G., Barmin, M. P., Ratnikova, L. I., and Its, E. N., 1989, Seismic surface waves in a laterally inhomogeneous earth: edited by V. I. Keilis-Borok, Springer, New York.

Luo, Y., Yang, Y., Xu, Y., Xu, H., Zhao, K., and Wang, K., 2015, On the limitations of interstation distances in ambient noise tomography: Geophysical Journal International, **201**, No. 2, 652–661.

Mac Dowell, N., Fennell, P., Shah, N., and Maitland, G., 2017, The role of $CO_2$ capture and utilization in mitigating climate change: Nature Climate Change, 7/243.

Macquet, M., Lawton, D. C., Saeedfar, A., and Osadetz, K. G., 2019, A feasibility study for detection threshold of co2 at shallow depths at the cami field research station, newell county, alberta, canada: Petroleum Geoscience, petgeo2018–135.

Mainsant, G., Larose, E., Brönnimann, C., Jongmans, D., Michoud, C., and Jaboyedoff, M., 2012, Ambient seismic noise monitoring of a clay landslide: Toward failure prediction: Journal of Geophysical Research: Earth Surface, **117**, No. F1.

Mao, S., Campillo, M., van der Hilst, R. D., Brenguier, F., Stehly, L., and Hillers, G., 2019, High temporal resolution monitoring of small variations in crustal strain by dense seismic arrays: Geophysical Research Letters, **46**, No. 1, 128–137.

Marchesini, P., Daley, T. M., and Nihei, K., 2019, Updates on crosswell seismic tomographic surveying ar CaMI-FRS: Containment and Monitoring Institute and CMC Research Institutes Suscriber workshop.

Marchesini, P., Daley, T. M., Wilt, M., Nichols, E., Um, E., and Cook, P., 2018, Baseline data for crosswell seismic and electromagnetics at CaMI: Containment and Monitoring Institute and CMC Research Institutes Suscriber workshop.

Meier, U., Shapiro, N., and Brenguier, F., 2010, Detecting seasonal varitions in seismic velocities winthin los angeles basin from correlations on ambient seismic noise: Geophysical Journal Interntional, **181**, No. 985-996.

Mordret, A., Landès, M., Shapiro, N., Singh, S., Roux, P., and Barkved, O. I., 2013, Near-surface study at the valhall oil field from ambient noisesurface wave tomography: Geophysical Journal International, **193**, No. 3, 1627–1643.

Obermann, A., 2013, Monitoring the elastic properties of the crust: numerical analysis and applications using ambient seismic noise: Ph.D. thesis, ISTerre (Institut des Sciences de la Terre).

Obermann, A., Kraft, T., Larose, E., and Wiemer, S., 2015, Potential of ambient seismic noise techniques to monitor the St. Gallen geothermal site (Switzerland): Journal of Geophysical Research: Solid Earth.

Olivier, G., and Brenguier, F., 2016, Interpreting seismic velocity changes observed with ambient seismic noise correlations: Interpretation, **4**, No. 3.

Olivier, G., Brenguier, F., Carey, R., Okubo, P., and Donaldson, C., 2019, Decrease in seismic velocity observed prior to the 2018 eruption of kīlauea volcano with ambient seismic noise interferometry: Geophysical Research Letters, **46**, No. 7, 3734–3744.

Qu, L., Innanen, K., and Dettmer, J., 2019, DAS data processing using transdimensional inversion method: CREWES Research Report, **this volume**.

Ratdomopurbo, A., and Poupinet, G., 1995, Monitoring a temporal change of seismic velocity in a volcano: Application to the 1992 eruption of Mt. Merapi (Indonesia): Geophysical research letters, **22**, No. 7, 775–778.

Rippe, D., Schmidt-Hattenberger, C., and Lettow, H., 2017, Electrical resistivity tomography measurements at the field research station near brooks, alberta, canada (september 19 – september 22, 2016): CaMI Research Report, **2**.

Rippe, D., Strom, A., and Schmidt-Hattenberger, C., 2016, Electrical resistivity tomography baseline repeat at the field research station near brooks, alberta, canada (september 26 – october 4, 2017): CaMI Research Report, **1**.

Rostron, B., White, D., Hawkes, C., and Chalaturnyk, R., 2014, Characterization of the aquistore $CO_2$ project storage site, Saskatchewan, Canada: Energy Procedia.

Shapiro, N., and Campillo, M., 2004, Emergence of broadband Rayleigh waves from correlations of the ambient seismic noise: Geophysical Research Letters, **31**, No. 7.

Spackman, T. W., and Lawton, D. C., 2017, Seismic monitoring with continuous seismic sources: CREWES Research Report, **29**.

Spackman, T. W., and Lawton, D. C., 2018, Processing and analysis of data recorded from a buried permanent seismic source: CREWES Research Report, **30**.

Storke, A., Kendall, M., Kendall, R., Horleston, A., and Goble, D., 2018, Boradband monitoring at FRS - baseline results: Containment and Monitoring Institute and CMC Research Institutes Suscriber workshop.

Withers, M., Aster, R., Young, C., Beiriger, J., Harris, M., Moore, S., and Trujillo, J., 1998, A comparison of select trigger algorithms for automated global seismic phase and event detection: Bulletin of the Seismological Society of America, **88**, No. 1, 95–106.